DRONE-BASED CORROSION DETECTION ON HIGH-VOLTAGE TRANSMISSION TOWERS BASED ON SPECTRAL ANGLE CLASSIFICATION AND CLUSTERING

Rafał Muszyński[1], *Gonzalo Luzardo*[1], *Zohreh Zahiri*[2], *Roeland Vandebriel*[2]
Michiel Vlaminck[1], *Ljiljana Platisa*[1], *Frédéric Mangialetto*[3], *Hiep Luong*[1]

(1) IPI-URC-imec, Ghent University, Ghent, Belgium;
(2) Imec, Kapeldreef 75, 3001 Heverlee, Belgium;
(3) Elia, Brussels, Belgium

ABSTRACT

To evaluate the remaining lifetime of high voltage metallic towers, continuous inspections are required. These inspections are done today by experts climbing the towers, which is not only risky and time-consuming, but also costly and limited (not all parts of the towers can be reached). Hence, it is very important to develop an alternative inspection method to properly assess the repair these towers needs and extend their lifetimes. Imaging from drones is considered as a safe and fast tool for monitoring the environment and assets. However, using RGB imaging, it is not possible to distinguish between various types of corrosions, some of which can lead to severe material loss and thus compromised structural integrity. Moreover, RGB based image analysis is prone to false positives. Although hyperspectral imaging solves some of those problems, varying illumination conditions outdoor and the complex geometry of the towers bring extra challenges, which are addressed in the methodology developed in this paper. We designed a drone payload integrating both a LiDAR scanner and hyperspectral sensors. Leveraging reference spectra captured during a manual initialization step and extra features such as high dynamic range (HDR) for hyperspectral image acquisition resulted in a faster, less complex, and more reliable corrosion inspection.

Index Terms— hyperspectral imaging, corrosion detection, LiDAR, UAV, metallic towers

1. INTRODUCTION

The high-voltage towers in Belgium are progressively getting close to their operational end of life. More than 3000 towers were installed by Elia in the 1930s and will be reaching the age of 100 years by 2030. Estimating the remaining lifetime of these towers, requires very sensitive and meticulous inspections. RGB imaging from drones can fail in the existence of other surface anomalies that are visually similar to corrosion.

In our previous study described in [1], we investigated the use of imec's VIS-NIR hyperspectral cameras on a UAV payload to detect and differentiate corrosion on high-voltage towers. Continuing this research, we encountered several challenges that affected the effectiveness of our proposed pipeline in more complex real-life scenarios. These challenges include generating a point cloud of the tower using low-resolution hyperspectral images and creating luminance masks from unaligned exposure images due to hardware limitations with respect to capturing different exposures simultaneously, among others. These challenges impacted the reliable application of our pipeline. Capturing high-quality images to create an accurate point cloud of the tower, which is essential for accurate segmentation and corrosion location estimation, proved to be particularly challenging in practice.

In response to the described challenges, we improved our payload and pipeline as follows: i) we replaced the 25 mm lenses of the hyperspectral camera with 50 mm lenses, allowing for a closer view of the tower; ii) we performed demosaicing to obtain high-resolution hyperspectral images; iii) we simplified our approach for corrosion detection by incorporating a manual initialization step to enhance robustness; iv) we added a step for filtering and clustering corrosion in 3D space and made a preliminary estimation of the corrosion location on the tower; and v) we included a LiDAR sensor in our payload to investigate if the LiDAR data can help reconstruct a more accurate and complete point cloud of the tower.

2. RELATED WORK

Similar studies to detect corrosion using drone images have been conducted in the past. For example, CorrDetector [2] uses convolutional neural networks to detect corrosion on drone-captured RGB images of telecommunication towers. In [3], Ortiz et al. utilized micro-aerial vehicles with RGB cameras to perform corrosion detection on vessels. However, approaches based on RGB images are more prone to false positives. Additionally, using RGB images makes it difficult to differentiate between different degrees of corrosion, which is crucial for estimating the remaining lifetime of the towers.

Other studies on hyperspectral imaging for corrosion de-

tection have also shown promising results. For example, research by Thomas and Gündel [4] and Zahiri et al. [5] analysed a wide range of wavelengths, from 300nm to 2500nm, for corrosion detection on steel. We work with data captured in situ with drones and describe challenges faced in real-life applications.

This paper continues the work described in [1, 6]. Here, we present changes we made to our previous approach, aiming to improve results and robustness in more complex real-life scenarios. From the hardware side, we updated our payload by including new lenses and a LiDAR sensor for robust point cloud estimation. To reduce reliance on assumptions and the quality of foreground-background segmentation, we introduced a more robust manual initialization step. Subsequently, we designed a nearest neighbor classifier that leverages information from the initialization step. Furthermore, we reprojected corroded pixels estimated from images captured at different exposure times onto the tower surface. These projected 3D pixels were further analyzed and filtered to remove outliers.

3. MATERIAL AND METHODS

We updated our payload with a major component, an Ouster OS1-128 LiDAR sensor. Other changes include new 50 mm lenses to provide a closer view of the tower. In summary, our new payload now consists of two imec hyperspectral snapshot cameras (VIS and NIR), a 128-beam Ouster OS1 LiDAR sensor, and an SBG Quanta GNSS/IMU system to aid the point cloud reconstruction.

The VIS and NIR cameras feature 4x4 mosaic filter arrays, yielding 16 and 15 bands after calibration, respectively, covering wavelengths from 470nm to 860nm. The Ouster OS1 LiDAR sensor is controlled by the CPU included in the imec hyperspectral camera (NVIDIA Jetson board). The Ouster LiDAR scanner has 128 scan lines, a horizontal field of view (FOV) of 360°, and a vertical FOV of 45°. Synchronization with the IMU is achieved by time-stamping each laser beam firing. We adapted the hardware and software components of the payload to synchronize the LiDAR and hyperspectral data. The payload was mounted on a Gremsy Gimbal T7, as illustrated in Figure 1.

The processing pipeline is divided into four main components: i) preprocessing of RAW data, ii) point cloud estimation and segmentation, iii) corrosion classification, and iv) reprojection and clustering.

3.1. Hyperspectral data processing

The aim of this step is to restore hyperspectral cubes from snapshot mosaic imaging data. In our previous approach, we included several steps, such as dark noise correction, demosaicing, radiometric correction, angular correction, and non-uniformity correction. However, in our new approach, which incorporates a manual initialization to obtain reference spectra for the tower and corrosion, these correction steps are not required. Therefore, our processing is mainly focused on demosaicing RAW data to obtain a high-resolution hyperspectral image, facilitating the detection of small corrosion spots and achieving robust 3D reconstruction. Demosaicing is accomplished using a convolutional network. Since there is no dataset containing ground truth for the demosaicing task of our sensors, we train our network on synthetic data.

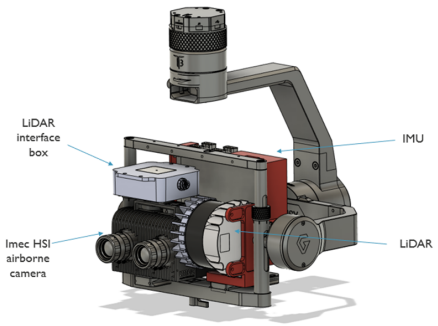

Fig. 1: 3D design of the imec hyperspectral and LiDAR integrated sensors for UAV payload

Our system should be able to adapt to varying light conditions (for example due to cloudy weather) as well as possible shadows (caused by self occlusion), and still be able to capture a well exposed image, with good contrast, of each part of the tower. Therefore, the hyperspectral camera was configured to take three exposures of approximately the same scene (a section of the electricity tower). The user only needs to set the base integration time for correct exposure, determining acceptable levels of overexposed and underexposed regions. The camera then captures two additional exposures: one with half the base exposure integration time (under-exposed image) and the other with double the base exposure integration time (over-exposed image). This method extends the dynamic range of the captured scene, enabling the acquisition of information in both over-exposed and under-exposed tower sections.

3.2. Point cloud estimation and segmentation

LiDAR and IMU data are processed to compute a 3D point cloud of the tower. For this, we used our proposed point cloud registration method detailed in [7], which involves two steps. First, scan-to-scan alignment aligns two consecutive point clouds, providing an initial estimate of the sensor's relative pose. The second point cloud is transformed using this estimate and the previously computed pose (dead reckoning) to place it in the world coordinate system. Then, scan-to-map alignment is performed between the transformed point cloud and the aggregated point cloud.

As in our previous approach, the segmentation of the

tower from other elements in the scene relies on estimating the depth for every pixel in the hyperspectral image. Closer pixels are considered as part of the tower; otherwise, they are considered as background. Depth estimation was achieved using multi-view stereopsis (MVS). For this, we required the camera poses as input, which were computed using a Structure from Motion (SfM) pipeline based on open-source algorithms from COLMAP [8]. Since the resulting hyperspectral cubes from demosaicing cannot be used directly with these algorithms, we convert the cubes into false-color RGB images. This conversion is performed by selecting three bands (3,12,16), normalizing them, and applying gamma correction.

3.3. Corrosion classification improvement

Due to the impracticality of using reference panels, our pipeline operates with radiance data, necessitating a reference for interpreting the observed spectra. To address this, we propose a simple manual initialization step to mark corrosion-free and, if possible, corroded pixels on one of the captured images. Using these annotations from a single image, our spectral angle-based predictor performs corrosion detection across the entire tower. Currently, we only use VIS data. We leave NIR integration as future work.

3.3.1. Manual initialization

Figure 2 shows the graphical user interface (GUI) used for manual initialization. The user annotates corrosion-free and, if present, corroded parts of the tower. The GUI assists the user in making optimal annotations by displaying current detection results. Additionally, a slider is included in the GUI to control the decision thresholds for the classifier.

3.3.2. Corrosion detection

This process is conducted on segmented hyperspectral pixels belonging to the tower, obtained from the high-resolution cubes after demosaicing. As a preprocessing step, each band of the demosaicked cube is smoothed with a 3×3 box blur to reduce noise.

Our model collects information from user annotations, categorizing them as corroded (positive samples) and uncorroded (negative samples) spectra. Then, hyperspectral pixels in all input images are classified based on three features: i) the nearest sample in terms of angular distance, ii) the value of the angular distance to the nearest sample, and iii) information from the false-color image.

First, our algorithm uses the angular distance to the nearest negative sample (uncorroded). If this distance is greater than a predefined threshold (2 degrees in our experiments), the pixel is marked as possible corrosion that needs further analysis. Specifically, our algorithm marks all outliers as candidates for corrosion. Additionally, if positive samples (corroded) are available, the pixel marked as possible corrosion in the first step is assigned to the class of the nearest sample. This pixel is considered corroded only if the distance to the nearest positive sample is smaller than a predefined threshold (4 degrees in our experiments). This second condition helps filter out false-positive detections. Finally, we use false-color images to filter out possible corrosion candidates that do not meet certain color criteria. Assuming that rust is dark, or contains brown/reddish color tones, we remove corrosion pixels that do not correspond to this color range. This task is conducted in the HSV color space, which allows for more direct and robust color comparisons. Specifically, corrosion pixels must meet the following criteria: Hue < 60 or Value < 125. These thresholds were empirically defined in our experiments.

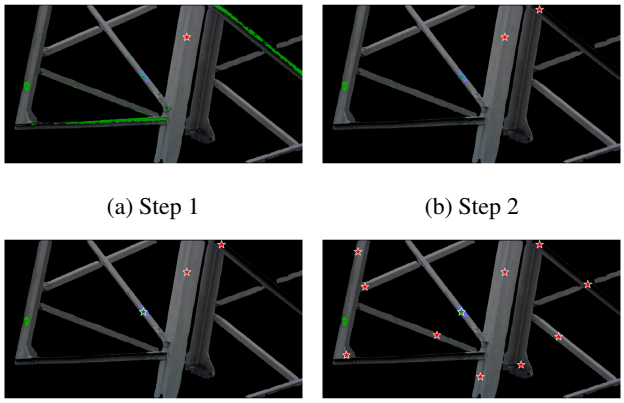

(a) Step 1 (b) Step 2

(c) Step 3 (d) Step 4

Fig. 2: Initial annotation steps. User annotations are marked with red stars for uncorroded pixels and green stars for corroded pixels. In steps 1-2, the user annotates pixels without any corrosion. The model's predictions are instantly displayed in green to guide the user on areas where the model still struggles. In steps 3-4, the user additionally provides possible corrosion locations, further enhancing the model's predictions. In the figure, blue marks indicate possible corrosion spots.

3.4. Reprojection and clustering

For each image, pixels identified as corrosion are re-projected onto the point cloud of the electricity tower. Only points that intersect with the point cloud are considered valid. This eliminates small segmentation errors that mistakenly classify background pixels as corrosion. Finally, the points are grouped into clusters using the DBSCAN algorithm [9]. Assuming that true corrosion pixels are consistently identified in most images captured with different integration times, unlike shadows and other elements, clusters with a lower density of 3D points within the volume they occupy are considered outliers.

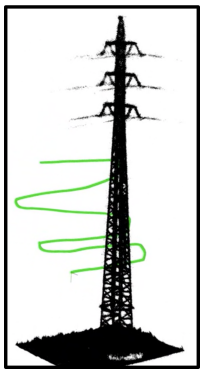

Fig. 3: Point cloud created using LiDAR data. The green line represents the drone's trajectory used for capturing.

(a) (b) (c)

Fig. 4: Corrosion detection - zoomed-in results paired with reference RGB images. Green marks predictions, while blue roughly outlines possible corrosion regions.

4. RESULTS

The evaluation of our proposed approach was conducted using data captured with our new payload from electric towers located near Kluisbergen, Belgium.

As a first step, we processed the data captured by the LiDAR and IMU to create a point cloud of electrical towers. As shown in Figure 3, the entire electrical tower can be reconstructed in good detail. Although the point cloud is not very dense, the obtained result is better than results obtained from VIS camera. We estimate that it is more than sufficient to estimate the location of the corrosion points accurately.

To evaluate corrosion detection on real captured data, we selected sample VIS images of 3 different towers, which we annotated based on RGB images with rough masks showing possible corrosion locations. For the initial corrosion detection tests, we manually created foreground masks.

Figure 4 presents corrosion detection results on our sample images. As can be seen in figures 4a and 4a, many corrosion spots are detected using our approach. Depending on the initial annotation steps, different false positives can appear in the final predictions, see Figure 4c.

Overall, the obtained masks are still noisy and contain

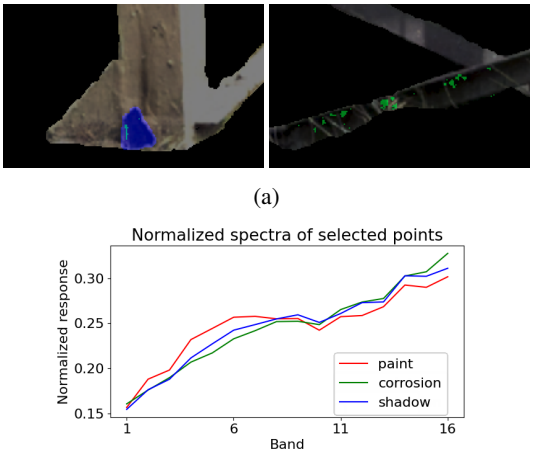

(a)

(b)

Fig. 5: Corrosion detection - challenging cases. Shadow and corrosion regions are very similar which leads to false positive detections

many false positives. Shadow areas are still problematic using our approach. Figure 5 presents a more challenging scenario. In this case, despite best annotating efforts, shadows are still marked as corrosion. Moreover, annotating shadows as a negative sample, leads to weak prediction on the actual corrosion. While high exposure time reduces dark areas, still some areas are not well visible. Figure 5b presents spectra in an image with the longest exposure time.

To analyse the results quantitatively, we calculate the following metrics:

- False discovery rate (FDR): # False positive pixels / # Pixels with positive predictions. This number expresses how trustworthy the model's predictions are.
- False positive rate (FPR): # False positive pixels / # Corrosion free pixels. This number expresses the percentage of falsely marked corrosion free pixels.
- Corrosion spot detection rate (SDR): # Detected spots / # Annotated possible corrosion spots. This number expresses the percentage of detected spots. We mark a spot as detected, if at least one pixel within our annotation is marked as corrosion.
- Positive rate (PR): # Positive pixels / # Tower pixels. This number expresses what percentage of tower is marked as corroded.

Table 1 presents quantitative results averaged per tower. We see that the classifier quality varies (FDR) and is very low in some cases (tower2). While not all of the spots were detected, this was not our goal, since some of them are possibly not corroded - manual tower inspection is required for final

FDR ↓	FPR ↓	SDR ↑	PR ↓	Tower
49 %	0.04 %	33 %	0.14 %	Tower 1
98 %	0.04 %	33 %	0.04 %	Tower 2
32 %	1.23 %	90 %	3.2 %	Tower 3

Table 1: Quantitative results of our experiments

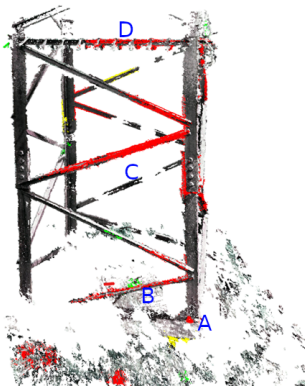

Fig. 6: 3D reconstructed section of a tower with predicted corrosion spots. Different colours mark different corrosion density, red being the most severe.

conclusions. Currently, major spots are detected, while the number of false positives is limited to a minimum.

To test the full pipeline, we selected all images from a section of one of the towers that we have captured in our data. Final results, marked on a 3D reconstruction are shown in Figure 6. The tower is reconstructed using only VIS images. Currently, ground is still not removed completely, which leads to false corrosion detections. Major corrosion spot at the bottom of the tower (A) (also seen in Figure 5a) is correctly marked as corrosion. Other possible corrosion spots (D) are marked as well. Unfortunately, multiple shadow areas are still marked as corrosion (B and C).

5. CONCLUSIONS

In this work, we present a complete pipeline for corrosion detection and localization on transmission towers. We demonstrate an effective usage of drone mounted LiDAR for accurate reconstruction of the tower. By collecting reference spectra from a single image, during the manual initialization step, we are able to successfully detect corrosion on the whole tower while keeping a low number of false positives. Our pipeline aggregates information from multiple hyperspectral images and combines it on a 3D model of the tower. Based on our experiments and captured data, our current work improves on previous approaches and brings us a step closer to fully automated drone based inspections.

Future work should concentrate on combining LiDAR and image based 3D reconstructions, incorporating NIR data for corrosion classification and improving corrosion prediction aggregation in 3D.

6. REFERENCES

[1] M. Vlaminck et al., "Drone-based corrosion detection on high-voltage transmission towers using hyperspectral imaging," in *2023 13th Workshop on Hyperspectral Imaging and Signal Processing: Evolution in Remote Sensing (WHISPERS)*. 2023, p. 5, IEEE.

[2] R. M. Abdur et al., "Corrdetector: A framework for structural corrosion detection from drone images using ensemble deep learning," *Expert Systems with Applications*, vol. 193, pp. 116461, 2022.

[3] Alberto Ortiz, Francisco Bonnin-Pascual, Emilio Garcia-Fidalgo, and Joan P. Company-Corcoles, "Vision-based corrosion detection assisted by a micro-aerial vehicle in a vessel inspection application," *Sensors*, vol. 16, no. 12, 2016.

[4] Dominik Thomas and Max Gündel, "Hyperspectral imaging systems for corrosion detection from remotely operated vehicles," *ce/papers*, vol. 6, no. 5, pp. 934–938, 2023.

[5] Zohreh Zahiri, Alfredo Lamberti, Jan Wielant, and Paul Scheunders, "Characterization of corrosion products on carbon steel using hyperspectral imaging in short-wave infrared (swir)," in *2022 12th Workshop on Hyperspectral Imaging and Signal Processing: Evolution in Remote Sensing (WHISPERS)*, 2022, pp. 1–4.

[6] Z. Zahiri et al., "Detecting and characterizing corrosion on high voltage metallic towers using hyperspectral imaging," in *2022 12th Workshop on Hyperspectral Imaging and Signal Processing: Evolution in Remote Sensing (WHISPERS), Abstracts*, 2022, p. 1.

[7] Michiel Vlaminck, Laurens Diels, Wilfried Philips, Wouter Maes, René Heim, Bart De Wit, and Hiep Luong, "A multisensor uav payload and processing pipeline for generating multispectral point clouds," *Remote Sensing*, vol. 15, no. 6, pp. 1524, 2023.

[8] Johannes Lutz Schönberger and Jan-Michael Frahm, "Structure-from-motion revisited," in *Conference on Computer Vision and Pattern Recognition (CVPR)*, 2016.

[9] Erich Schubert, Jörg Sander, Martin Ester, Hans Peter Kriegel, and Xiaowei Xu, "Dbscan revisited, revisited: why and how you should (still) use dbscan," *ACM Transactions on Database Systems (TODS)*, vol. 42, no. 3, pp. 1–21, 2017.